nature cell biology

In vitro contraction of cytokinetic ring depends on myosin II but not on actin dynamics

Mithilesh Mishra[1,5], Jun Kashiwazaki[2,5], Tomoko Takagi[2], Ramanujam Srinivasan[3], Yinyi Huang[3], Mohan K. Balasubramanian[1,3,4,6] and Issei Mabuchi[2,6]

Cytokinesis in many eukaryotes involves the contraction of an actomyosin-based contractile ring[1,2]. However, the detailed mechanism of contractile ring contraction is not fully understood. Here, we establish an experimental system to study contraction of the ring to completion *in vitro*. We show that the contractile ring of permeabilized fission yeast cells undergoes rapid contraction in an ATP- and myosin-II-dependent manner in the absence of other cytoplasmic constituents. Surprisingly, neither actin polymerization nor its disassembly is required for contraction of the contractile ring, although addition of exogenous actin-crosslinking proteins blocks ring contraction. Using contractile rings generated from fission yeast cytokinesis mutants, we show that not all proteins required for assembly of the ring are required for its contraction *in vitro*. Our work provides the beginnings of the definition of a minimal contraction-competent cytokinetic ring apparatus.

The understanding of biological processes benefits from the combined use of genetic analyses and *in vitro* reconstitution. Early studies in metazoan cells and embryos have established that an actomyosin-based contractile ring drives cytokinesis[3,4]. Isolation of the cleavage furrow containing the contractile ring has provided some structural information for the mechanism of cytokinesis[5], but the molecular components responsible for the supramolecular organization and function are not fully understood. Genetic analysis in various model organisms has succeeded in the identification of mutants defective in contractile ring assembly, characterization of which in turn has led to the identification of components of the contractile ring[1,2,6]. However, mutants defective specifically in ring contraction have not been identified, possibly because proteins involved in ring assembly might contribute to its contraction. As a result, the mechanism for ring contraction and disassembly is poorly understood. To circumvent the gaps in genetic analysis and to generate a thorough understanding of ring contraction we have sought to establish an *in vitro* system.

The fission yeast *Schizosaccharomyces pombe* divides by the use of a contractile ring and an invaginating septum[7,8]. Given the wealth of cytokinesis-defective mutants and the ease of using live-cell microscopy, we chose to establish the *in vitro* ring contraction system in this organism (Fig. 1a and Methods). We first removed the cell wall by enzymic digestion to obtain spheroplasts. Time-lapse imaging of mCherry–tubulin- and Rlc1p–3xGFP (myosin-II regulatory light chain)-expressing spheroplasts revealed that, like intact cells, spheroplasts assembled normal-appearing contractile rings[9] (Supplementary Fig. S1a,b). Then spheroplasts were permeabilized with 0.5% NP-40. The resultant cell ghosts retained a contractile ring (Fig. 1b) surrounded by plasma membrane full of holes as seen by FM4-64 staining and by thin-sectioning electron microscopy, but were devoid of any cytoplasmic structures (Fig. 1b,c). Most proteins necessary for contractile ring formation were contained in the contractile ring in cell ghosts (Fig. 1d–g and Supplementary Fig. S2a and Table S1) but other cytoplasmic components were not (Supplementary Fig. S2b and Table S1). Biochemical analysis showed that the ring components myosin-II, actin and tropomyosin Cdc8p were enriched in the ghost preparations, whereas tubulin was not (Fig. 1h and also Supplementary Fig. S2b).

To determine whether these rings were contractile, we treated cell ghosts with 0.5 mM ATP. Rings underwent rapid contraction on ATP addition (Fig. 2a,b and Supplementary Video S1). It has been reported that contractile rings isolated from spheroplasts of budding yeast disappeared on ATP addition, although the mechanisms were not explored[10]. As for the intact cells[11–13], the rate of contraction of rings from fission yeast cell ghosts was almost constant from initiation to completion, and was $0.22 \pm 0.09\ \mu m\ s^{-1}$ ($n = 37$; Fig. 2b). Contraction with a slightly reduced rate was observed even when the ATP concentration was as low as 0.01 mM (Fig. 2c and Supplementary Video S2), but not in the presence of the non-hydrolysable ATP analogue

[1]Temasek Life Sciences Laboratory, The National University of Singapore, 1 Research Link, Singapore 117604, Singapore. [2]Department of Life Sciences, Faculty of Science, Gakushuin University, 1-5-1 Mejiro, Toshima-ku, Tokyo, 171-8588, Japan. [3]Mechanobiology Institute, The National University of Singapore, 117543, Singapore. [4]Department of Biological Sciences, The National University of Singapore, 117411, Singapore. [5]These authors contributed equally to this work. [6]Correspondence should be addressed to M.K.B. or I.M. (e-mail: mohan@tll.org.sg or issei.mabuchi@gakushuin.ac.jp)

Received 13 August 2012; accepted 9 May 2013; published online 16 June 2013; DOI: 10.1038/ncb2781

© 2013 Macmillan Publishers Limited. All rights reserved.

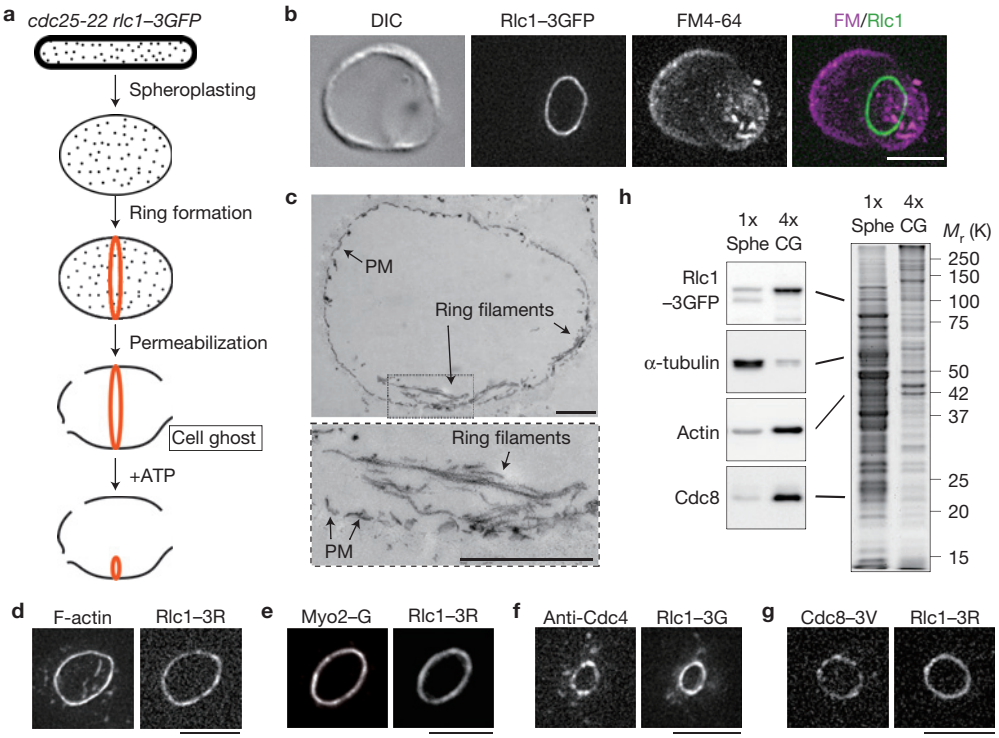

Figure 1 Contractile rings in cell ghosts. (**a**) Schematic illustration of procedure to obtain cell ghosts. (**b**) Maximum projection image of deconvolved sections of Rlc1–3xGFP and the plasma membrane stained with FM4-64 in a cell ghost. (**c**) A thin-section electron micrograph of the mid region of a cell ghost that is not parallel to the ring plane. Actin filaments in the ring were decorated with skeletal heavy meromyosin. The plasma membrane (PM) showed numerous gaps as a result of the detergent treatment. The area surrounded by a dotted rectangle is magnified below. (**d**) Maximum projection images of deconvolved sections of Rlc1–3xmDsRed and F-actin stained with BODIPY-FL–phallacidin in the cell ghosts. (**e**) Maximum projection images of deconvolved sections of Myo2–GFP and Rlc1–3xmDsRed. (**f**) Maximum projection images of deconvolved sections of Cdc4 stained with anti-Cdc4 antibody and anti-rabbit IgG labelled with tetramethylrhodamine after permeabilization and Rlc1–3xGFP. (**g**) Maximum projection images of deconvolved sections of Cdc8–3xVenus and Rlc1–3xmDsRed. (**h**) Western blot analysis of several proteins in the whole-cell lysate of spheroplasts (Sphe) or cell ghosts (CG). The density of cell ghosts was fourfold higher than that of spheroplasts. The right panel shows Coomassie-stained gels of total protein in spheroplasts and cell ghosts. Scale bars, 5 μm (**b**,**d**–**g**) and 1 μm (**c**).

AMP-PNP (Fig. 2d and Supplementary Video S3). The rate of ring contraction in cell ghosts in the presence of 0.5 mM ATP was more than 20 times faster than that in wild-type cells (Fig. 2e). The measurement of fluorescence of ring components over time revealed that whereas the total amount of most contractile ring proteins reduced only marginally, Cdc8p was rapidly depleted from the constricting ring (Fig. 2f and Supplementary Table S2). The fast rate of ring contraction *in vitro* may be a result of delinking of ring contraction from membrane and division septum assembly in cell ghosts as the associated membranes did not invaginate as the ring contracted (Fig. 2g and Supplementary Video S4). Although slow contraction was observed in the presence of other nucleoside triphosphates, the lowest K_m and highest V_m were observed for ATP (Fig. 2h,i). Thus, ring contraction in fission yeast requires ATP hydrolysis. Maximal ring contraction was observed at pH 8.0–8.5 with contraction being slower below pH 7 (Supplementary Fig. S3a). The optimal calcium concentration for ring contraction was pCa 8–9 and free Ca^{2+} lowered the contraction rate (Supplementary Fig. S3b), suggesting a Ca-sensitive step in ring contraction in fission yeast.

In time-lapse imaging of spheroplasts, contractile rings were routinely observed to initiate from a single location and occurred through what appeared as a bi-directionally growing leading cable[14] (Supplementary Fig. S1b). We established that this mode of bi-directional cable assembly was not a peculiarity of spheroplasts, because fission yeast cells rendered spherical also exhibited a similar ring assembly process (Supplementary Fig. S1c). Whereas fully formed rings underwent rapid ATP-dependent contraction, incomplete actomyosin arcs were unable to contract (Fig. 2j and Supplementary Video S5) although the fluorescence decayed significantly in the presence of ATP, which is probably due to disassembly (Supplementary Fig. S3c). This result is consistent with the observation that the forming ring consists of two semicircles of predominantly parallel F-actin filaments[15], which would not support ring contraction.

As the motor protein myosin-II hydrolyses ATP during its walking along an actin filament, we examined whether myosin-II activity was essential for ring contraction. Although myosin-II–actin interaction has been shown to be essential for cytokinesis[16], its molecular function in cytokinesis is not fully understood. We incubated cell ghosts in the presence of ATP and the myosin-II ATPase inhibitor blebbistatin (0.1 mM; ref. 17). Whereas rings underwent rapid contraction in the absence of blebbistatin, ring contraction was abolished in the presence of blebbistatin (Fig. 3a, $n=8$). We also found that incubation of cell ghosts with dehydroxestoquinone (DXQ; 2.5 mM), an inhibitor of skeletal muscle myosin II (ref. 18), and kinesin and dynein ATPases blocked ring contraction (Supplementary Fig. S3d,e). Treatment of cell ghosts with 0.1 mM sodium vanadate (an inhibitor of dynein and kinesin ATPases, but not myosin II ATPase) or microtubule-depolymerizing

© 2013 Macmillan Publishers Limited. All rights reserved.

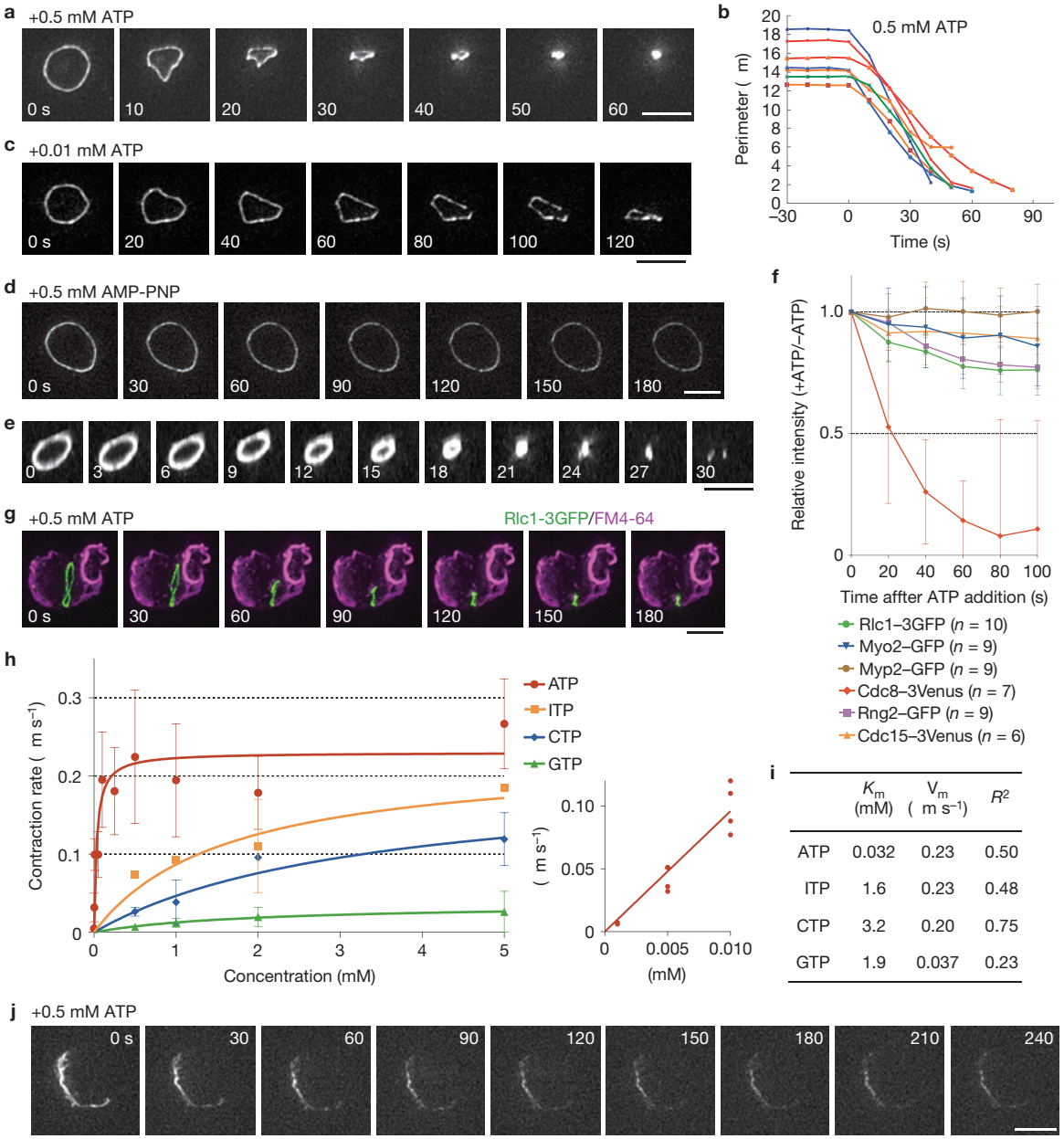

	K_m (mM)	V_m (m s^{-1})	R^2
ATP	0.032	0.23	0.50
ITP	1.6	0.23	0.48
CTP	3.2	0.20	0.75
GTP	1.9	0.037	0.23

Figure 2 ATP stimulates rapid ring contraction *in vitro*. Experiments were done at 25 °C. Fluorescence micrographs of Rlc1–3xGFP are shown as maximum projections of *Z*-stacks. (**a**,**b**) Ring contraction is stimulated on ATP addition *in vitro*. 0 s indicates time of ATP addition. Typical examples of time course of ring contraction are shown. Perimeters were measured after three-dimensional rotation (Methods). Each measured value is represented. (**c**) Ring contraction is slower in the presence of 0.01 mM ATP. (**d**) The ring does not contract in the presence of 0.5 mM AMP-PNP. (**e**) Ring contraction in a cylindrical wild-type fission yeast cell. Fluorescence micrographs of Rlc1–3xGFP are shown as 30°-tilted maximum projections of *Z*-stacks. (**f**) Disassembly of each ring component after 0.5 mM ATP addition. Fluorescence intensity is shown as the relative value to that in the absence of ATP to eliminate the effect of photobleaching. Each mean value is represented. For the values at 100 s, unpaired two-tailed *t*-tests were done. Each *P* value is shown in Supplementary Table S2. (**g**) The plasma membrane of Rlc1–3xGFP-expressing cell ghosts stained with FM4-64 during contraction *in vitro* in the presence of 0.5 mM ATP. (**h**,**i**) Nucleotide specificity for ring contraction *in vitro*. Actual values are shown in Supplementary Table S3. Each curve was fitted to the Michaelis–Menten equation. The small graph shows the rates at low concentrations of ATP. K_m and V_m were estimated using Prism-5. R^2 should be close to 1.0 if the curve is well fitted. Statistics source data for Fig. 2h can be found in Supplementary Table S6. (**j**) Incomplete contractile ring does not undergo ATP-driven contraction *in vitro*. ATP (0.5 mM) was added at 0 s. See Supplementary Videos S1–S5. Time is indicated in seconds (**a**,**c**,**d**,**g**,**j**) or minutes (**e**). Scale bars, 5 μm (**a**,**c**–**e**,**g**,**j**). Error bars represent s.d. (**f**,**h**).

drugs (methyl benzimidazol-2-yl-carbamate (MBC) and thiabendazole (TBZ)) did not affect ring contraction (Supplementary Fig. S4a). The inhibition of ring contraction by DXQ, but not by vanadate, MBC or TBZ, taken together with our results with blebbistatin strongly suggested that the ATPase activity of myosin II was essential for ring contraction.

We independently confirmed the role of myosin-II in ring contraction by preparing cell ghosts from myosin-II-mutant strains.

© 2013 Macmillan Publishers Limited. All rights reserved.

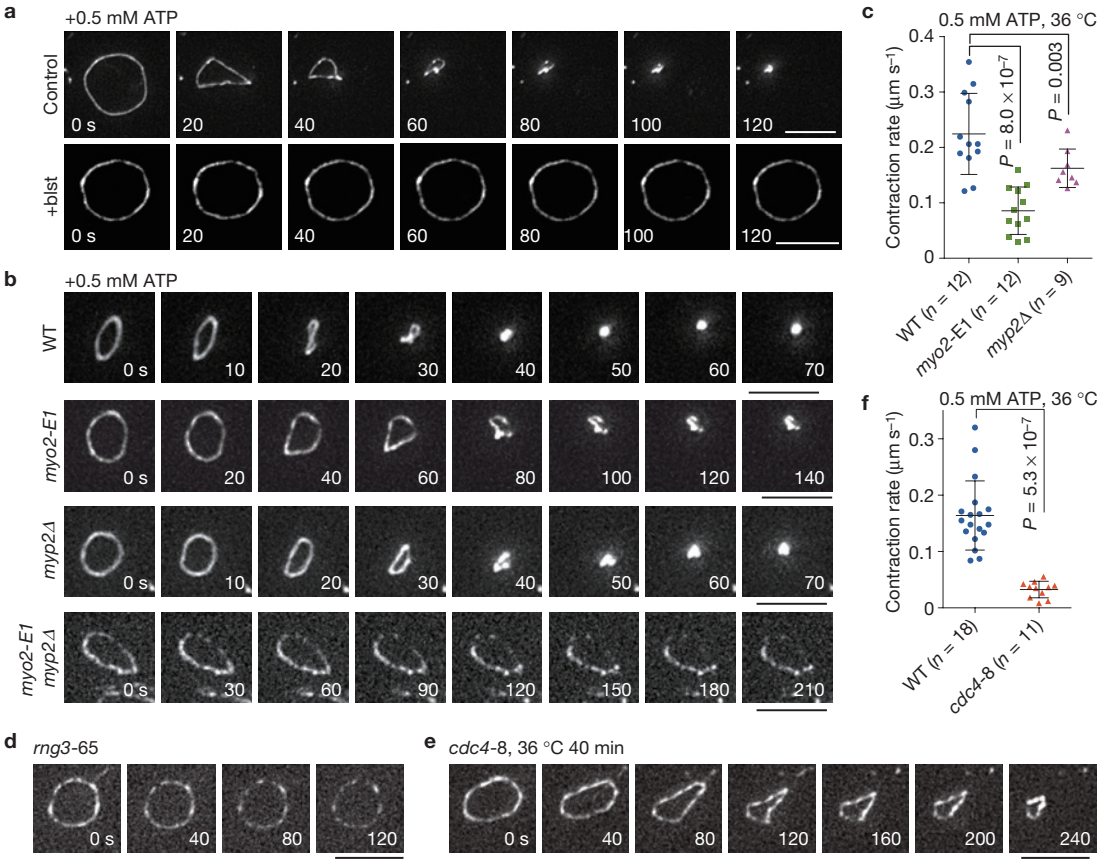

Figure 3 Myosin-II drives ring contraction *in vitro*. ATP concentration in each experiment was 0.5 mM. Fluorescence micrographs of Rlc1–3xGFP are shown as maximum projections of *Z*-stacks. (**a**) Effect of blebbistatin on ring contraction *in vitro*. Rings were pre-incubated in 0.1 mM blebbistatin for 3 min before perfusion with ATP (time 0 s) at 25 °C. (**b**) Rings in wild-type or myosin-II mutant cell ghosts. Ring contraction after ATP addition was monitored at the permissive temperature, 25 °C. (**c**) Contraction rate ($\mu m\,s^{-1}$) of contractile rings in myosin-II mutant cell ghosts at the permissive temperature. Each spot represents the rate of contraction of an individual ring. Medial horizontal lines and error bars represent mean values and s.d., respectively. Two-tailed *t*-test was used for statistical analysis. (**d**) Ring behaviour in *rng3*-65 mutant cell ghosts after ATP addition at the permissive temperature of 25 °C. (**e**) Ring contraction in *cdc4*-8 mutant cell ghosts 40 min after the temperature shift to 36 °C. (**f**) Contraction rate ($\mu m\,s^{-1}$) of rings in *cdc4*-8 mutant cell ghosts at the restrictive temperature. The graph is represented as in **c**. All scale bars, 5 μm. See Supplementary Videos S6–S8.

There are two genes that encode myosin-II heavy chain in fission yeast, essential *myo2*$^{+}$ (ref. 19) and non-essential *myp2*$^{+}$ (also known as *myo3*$^{+}$; refs 20,21). Spheroplasts were prepared from the temperature-sensitive (ts) mutant *myo2*-E1 (ref. 22), the *myp2*-null mutant (*myp2*Δ) and the *myo2*-E1 *myp2*Δ double-mutant grown at the permissive temperature of 25 °C. Mutant Myo2-E1p has been shown to have a reduced ATPase activity and an associated reduction in its motor activity even at the permissive temperature[23]. Rings in *myo2*-E1 or *myp2*Δ cell ghosts showed slower contraction even at 25 °C (Fig. 3b,c and Supplementary Videos S6 and S7). Most of the rings in *myo2*-E1 *myp2*Δ cell ghosts were either fragmented or deformed and these rings did not show any ATP-dependent contraction (Fig. 3b and Supplementary Video S8), suggesting that the contractile ring was not in a proper organization. Taken together, these experiments established that ATP hydrolysis by myosin-II powers the fission yeast ring contraction *in vitro*. Contractile rings in cell ghosts isolated from *rng3*-65^{ts} (defective in the UCS-domain-containing myosin-II activator and chaperone Rng3p; refs 23,24) were also unstable and did not undergo perceptible contraction even at 25 °C (17 out of 20 rings, Fig. 3d) even though they did retain all of the essential contractile ring proteins tested (Supplementary Table S4). Rings prepared from the myosin-II essential light chain mutant (*cdc4*-8^{ts}) underwent complex behaviour, ranging from very slow contraction to ring disintegration, possibly owing to the multiple roles performed by Cdc4p in cytokinesis[25] (Fig. 3e,f).

Previous studies in yeasts and animal cells have proposed the requirement for actin depolymerization and/or severing in ring contraction[3,26]. We first established that F-actin fluorescence was almost completely lost during ring contraction in cell ghosts (Fig. 4a,b). Using biochemical assays we found that on ATP addition to cell ghosts, actin was released from the ghosts (Fig. 4c,d). Myosin-II behaved differently, as most of it remained in the cell ghosts after ATP addition (Fig. 4e). This is consistent with the presence of myosin in a large spot following ring contraction on ATP addition (Figs 2a,f and 4a,b).

We next investigated whether this loss of F-actin was essential for ring contraction *in vitro*. To this end we first treated the cell ghosts with an F-actin-stabilizing drug jasplakinolide (Jasp). We found that on ATP addition ring contraction in cell ghosts occurred at normal

© 2013 Macmillan Publishers Limited. All rights reserved.

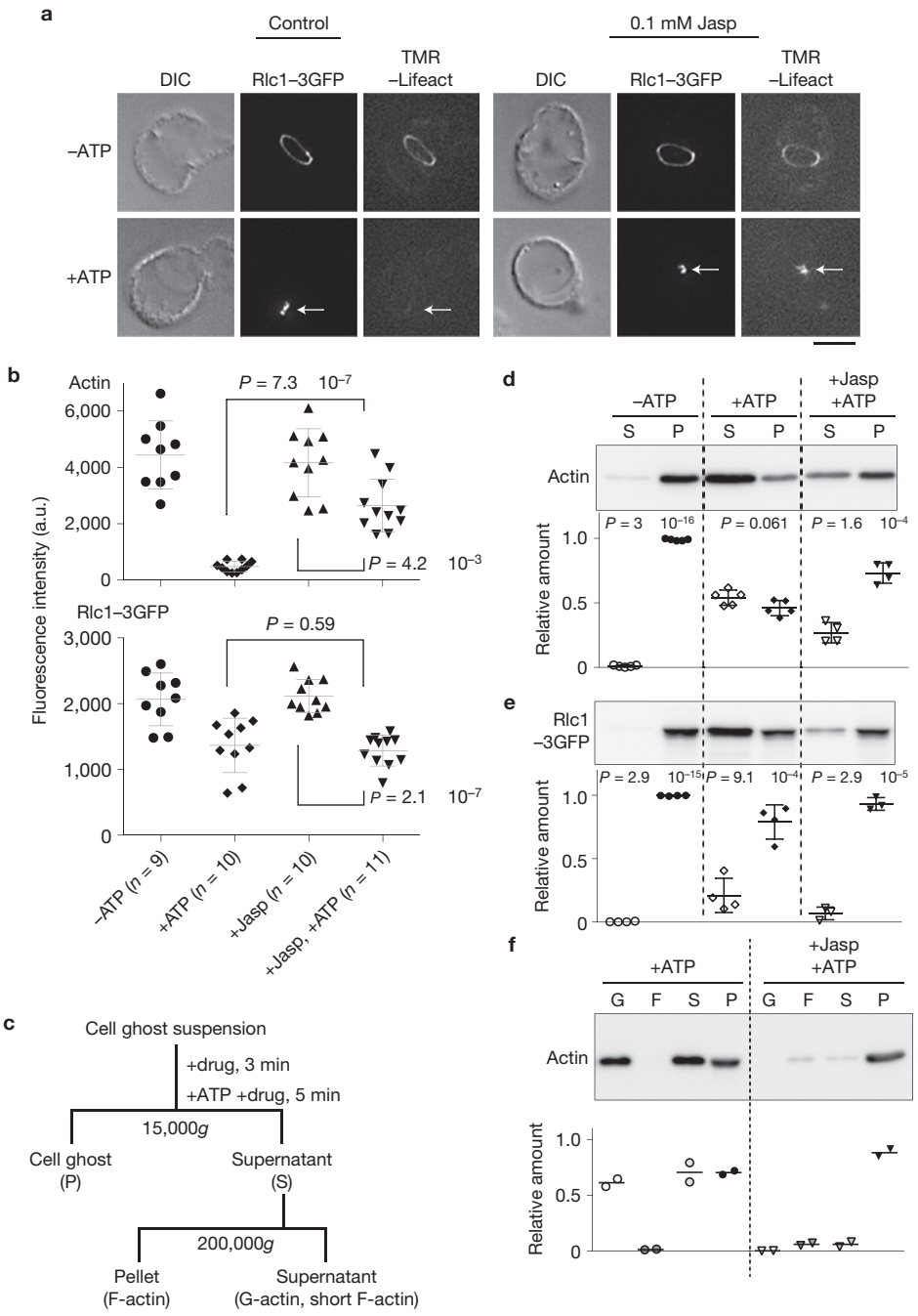

Figure 4 Contribution of actin dynamics to ring contraction *in vitro*. (**a**) Actin stabilization by Jasp does not block ring contraction. Actin was stained with 10 μg ml^{-1} TMR–Lifeact before or after contraction. White arrows indicate the positions of contracted rings. Scale bar, 5 μm. (**b**) Fluorescence intensity of TMR–Lifeact or Rlc1–3xGFP in contractile rings before and after ATP addition. Each spot represents the integrated intensity of actin or Rlc1–GFP in each contractile ring. Medial horizontal lines and error bars represent mean values and s.d., respectively. (**c**) Schematic flow chart of actin disassembly assay (Methods). (**d**,**e**) Western blot analysis of actin or Rlc1 disassembly on ATP addition in the absence or presence of Jasp. S, supernatant; P, pellet. Amount of pellet loaded is threefold lower than that of the corresponding supernatant. Each relative amount was calculated from the total intensity (S + P × 3). Statistics source data for **d**,**e** can be found in Supplementary Table S6. (**f**) Sedimentation assay of released actin on ATP addition in the absence or presence of Jasp. G, G-actin and short F-actin; F, F-actin. Amount of pellet loaded is one-and-a-half times lower than that of its supernatant. Each relative amount was calculated from the amount of actin in the pellet without ATP. Two-tailed *t*-test was used for all statistical analyses. Statistics source data for **f** can be found in Supplementary Table S6. All error bars represent s.d.

kinetics in the presence of 0.1 mM Jasp (Supplementary Fig. S4a and Video S9). Other F-actin stabilizers, phalloidin or phallacidin at 0.1 mM, also did not affect the rate of ring contraction (data not shown). Unlike in the contractile rings of untreated cells, actin filaments were readily visible in rings treated with Jasp, phalloidin or phallacidin (Fig. 4a,b and Supplementary Fig. S4c).

We reconfirmed the effect of Jasp, phalloidin or phallacidin treatment on actin stabilization by sedimentation assays. When ghosts

© 2013 Macmillan Publishers Limited. All rights reserved.

were treated with ATP and Jasp, most actin was still retained in the cell-ghost pellet, and a small fraction was released in the supernatant (Fig. 4c,d). By performing further sedimentation assays, we found that actin released into the supernatant in the presence of Jasp was largely composed of F-actin (Fig. 4c,f). This contrasts with ghosts treated with ATP alone, in which most actin detected in the supernatant might be monomeric (Fig. 4f). Similar results were obtained when phalloidin- or phallacidin-treated cell ghosts were biochemically characterized (Supplementary Fig. S4d). These results suggest that actin filament depolymerization is not required for ring contraction *in vitro*.

The small amount of actin filaments released during ring contraction *in vitro* suggested that, although actin filament depolymerization and monomer release were not required for this process, actin severing might be important. We therefore examined whether the F-actin-severing protein ADF/cofilin Adf1p, which is known to function in actin turnover and contractile ring formation[27], plays an essential role in ring contraction. Rings in *adf1*-1^{ts} cell ghosts contracted at rates comparable to those in the wild type at 36 °C (Supplementary Fig. S4b and Video S10). These results implied that actin severing by ADF/cofilin was not required for ring contraction *in vitro*. The experiments with Jasp and the *adf1*-1^{ts} mutant collectively established that neither actin severing nor depolymerization was essential for ring contraction *in vitro*.

It has been proposed that actin polymerization itself might generate the force required for ring contraction[12]. We directly examined whether actin polymerization was required for contractile ring contraction by pre-incubation of cell ghosts with the actin polymerization inhibitor latrunculin A (LatA) or cytochalasin A (CytA) before ATP addition. These rings contracted at a rate comparable to that of the control (Supplementary Fig. S4a and Video S11). The formin Cdc12p is an actin nucleator essential for cytokinesis[28,29]. The F-BAR domain protein Cdc15p recruits Cdc12p to the division site[30]. Contractile rings in cell ghosts of both *cdc12*-112^{ts} mutants and *cdc15*-140^{ts} mutants incubated at the restrictive temperature underwent normal contraction (Supplementary Fig. S4b and Videos S12 and S13). Contractile ring in cell ghosts of *cdc3*-124^{ts} cells (defective in the formin-binding protein profilin)[7] also contracted at wild-type rates (Supplementary Fig. S4b). Taken together these experiments demonstrated that actin polymerization was not essential for ring contraction.

We then tested investigated whether yeast tropomyosin Cdc8p is required for ring contraction. Cdc8p is essential for cytokinesis and is known to regulate actin stability and modulate actomyosin interaction, possibly by competing with fimbrin Fim1p and/or Adf1p for binding to actin filaments[27,31,32]. Contractile rings in *cdc8*-110^{ts} cell ghosts were capable of undergoing ATP-dependent contraction at the permissive temperature ($n = 5$, data not shown). Although these rings retained most essential contractile ring components at the restrictive temperature (Supplementary Table S4) they became discontinuous and did not contract to completion at the restrictive temperature (8 out of 9 rings, Fig. 5a and Supplementary Video S14). Thus, we concluded that Cdc8p is required for ring integrity during contraction.

The contractile ring contains F-actin-crosslinking proteins α-actinin Ain1p, the IQGAP Rng2p and Fim1p (refs 33–35), which are essential for proper organization of the actin bundles in the ring. We investigated whether an excess of actin crosslinker(s) impeded ring contraction by addition of these actin-crosslinking proteins to the cell ghosts

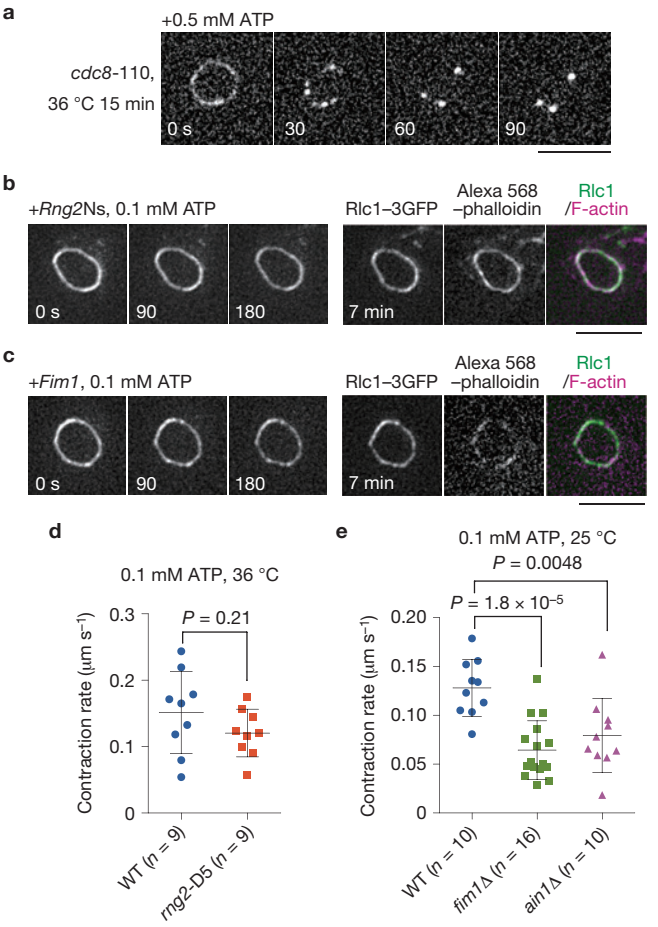

Figure 5 Effect of tropomyosin and actin-crosslinking proteins on ring contraction *in vitro*. (**a**) Ring behaviour in *cdc8*-110 mutant cell ghosts 15 min after the temperature shift to 36 °C. Fluorescence micrographs of Rlc1–3xGFP are shown as maximum projections of *Z*-stacks. ATP concentration was 0.5 mM. (**b**,**c**) Addition of purified amino-terminal region of IQGAP (Rng2Ns, 1 μM) or fimbrin (Fim1, 0.9 μM) blocks ring contraction *in vitro*. ATP concentrations were 0.1 mM. F-actin was stained with Alexa 568–phalloidin 7 min after ATP addition. (**d**) Contraction rate of rings in *rng2*-D5 mutant cell ghosts 40 min after the temperature shift to 36 °C. (**e**) Contraction rates of rings in *fim1*Δ and *ain1*Δ cell ghosts at 25 °C. All scale bars, 5 μm. Each spot represents the rate of contraction of an individual ring. Medial horizontal lines and error bars represent mean values and s.d., respectively. Two-tailed *t*-test was used for statistical analysis. See Supplementary Videos S9–S16.

before ATP addition. When cell ghosts were pre-incubated with purified Rng2Ns possessing the actin-bundling activity[35], contraction was blocked in a dose-dependent manner with a complete block at 1 μM ($n = 4$, Fig. 5b and Supplementary Fig. S5a and Video S15), a concentration that promoted robust actin filament bundling *in vitro* (Supplementary Fig. S5c). Phalloidin staining of these rings showed that actin filaments remained in the ring (Fig. 5b). Fim1p showed a similar dose-dependent inhibition of ring contraction *in vitro* with 0.9 μM Fim1p completely blocking ring contraction ($n = 3$, Fig. 5c and Supplementary Fig. S5b and Video S16). To determine whether a defect or absence of each crosslinker caused an increase in ring contraction rate, we prepared ghosts from *rng2*-D5^{ts} mutant cells or cells deleted for *fim1*$^{+}$ or *ain1*$^{+}$. Curiously, rings from *rng2*-D5^{ts}

© 2013 Macmillan Publishers Limited. All rights reserved.

spheroplasts contracted at a normal rate at 36 °C, and in the absence of Fim1p or Ain1p rings showed a slower rate of contraction (Fig. 5d,e). These experiments suggested that a balance of activity of crosslinking proteins was essential for proper ring contraction.

We have established an *in vitro* contractile ring activation system in which we have shown that fully formed contractile rings, but not partially formed arcs, undergo ATP-dependent contraction. The fact that the rings in cell ghosts undergo rapid contraction establishes that neither a constant supply of cytoplasmic material nor the concomitant ingression of septum is required for the mechanics of ring contraction in fission yeast. Our analysis, using this *in vitro* approach, therefore leaves us with the minimal requirements for ring contraction; namely, F-actin, myosin-II ATPase and the appropriate actin-crosslinking. □

METHODS

Methods and any associated references are available in the online version of the paper.

Note: Supplementary Information is available in the online version of the paper

ACKNOWLEDGEMENTS

We thank D. McCollum (University of Massachusetts Medical School, USA), K. Gould (Vanderbilt University, USA), J-Q. Wu (Ohio State University, USA), V. Simanis (ISREC, Switzerland), J. Bähler (University College London, UK), T. D. Pollard (Yale University, USA), T. Toda (Cancer Research, UK), I. Hagan (Paterson Institute, UK), F. Chang (Columbia University, USA), D. Mulvihill (University of Kent, UK), P. Perez (CSIC, Spain), Y. Hiraoka (Osaka University, Japan), K. Nakano (University of Tsukuba, Japan), S. Oliferenko (TLL, Singapore), and M. Sato (Waseda University, Japan) and the Yeast Genetic Resource Center Japan for providing plasmids and strains, Y. Oba and M. Ojika (Nagoya University, Japan) for their kind gift of DXQ, Y. Toyoshima (University of Tokyo, Japan) for her kind gift of kinesin, R. Amikura for help in electron microscopy, and S. Oliferenko, S. Bulchand and D. Subramanian for critical reading of this manuscript. We thank K. Gull (Oxford University, UK) for antibodies. We thank M. Sevugan for technical assistance. This work was supported by a Japan Society for Promotion of Science (JSPS) grant-in-aid for scientific research (I.M., #22247031); JSPS research fellowships for young scientists (J.K.); NUS JSPS collaborative grant (I.M. and M.B.), Temasek Life Sciences Laboratory and Singapore Millennium Foundation (M.B. and M.M.); visiting scientist fellowship from the Gakushuin University (M.M.) and Mechanobiology Institute (M.B., R.S. and Y.H.).

AUTHOR CONTRIBUTIONS

I.M. (*in vitro* activation and biochemistry) and M.K.B. (establishment of ring assembly in protoplasts and mutant studies) conceived the study, I.M., M.M., M.K.B. and J.K. designed the experiments. I.M., J.K., M.M., T.T., R.S. and Y.H. conducted the experiments. J.K., I.M. and M.M. analysed the data. M.K.B., M.M., J.K. and I.M. wrote the manuscript.

COMPETING FINANCIAL INTERESTS

The authors declare no competing financial interests.

Published online at www.nature.com/doifinder/10.1038/ncb2781
Reprints and permissions information is available online at www.nature.com/reprints

1. Glotzer, M. The molecular requirements for cytokinesis. *Science* **307,** 1735–1739 (2005).
2. Pollard, T. D. Mechanics of cytokinesis in eukaryotes. *Curr. Opin. Cell Biol.* **22,** 50–56 (2010).
3. Mabuchi, I. Biochemical aspects of cytokinesis. *Int. Rev. Cytol.* **101,** 175–213 (1986).
4. Schroeder, T. E. in *Molecules and Cell Movements* (eds Inoué, S. & Stephens, R. E.) 305–334 (Raven, 1975).
5. Mabuchi, I., Tsukita, S., Tsukita, S. & Sawai, T. Cleavage furrow isolated from newt eggs: contraction, organization of the actin filaments, and protein components of the furrow. *Proc. Natl Acad. Sci. USA* **85,** 5966–5970 (1988).
6. Robinson, D. N. & Spudich, J. A. Mechanics and regulation of cytokinesis. *Curr. Opin. Cell Biol.* **16,** 182–188 (2004).
7. Pollard, T. D. & Wu, J. Q. Understanding cytokinesis: lessons from fission yeast. *Nat. Rev. Mol. Cell Biol.* **11,** 149–155 (2010).
8. Wolfe, B. A. & Gould, K. L. Split decisions: Coordinating cytokinesis in yeast. *Trends Cell Biol.* **15,** 10–18 (2005).
9. Mishra, M. *et al.* Cylindrical cellular geometry ensures fidelity of division site placement in fission yeast. *J. Cell Sci.* **125,** 3850–3857 (2012).
10. Young, B. A., Buser, C. & Drubin, D. G. Isolation and partial purification of the Saccharomyces cerevisiae cytokinetic apparatus. *Cytoskeleton* **67,** 13–22 (2010).
11. Motegi, F., Arai, R. & Mabuchi, I. Identification of two type V myosins in fission yeast, one of which functions in polarized cell growth and moves rapidly in the cell. *Mol. Biol. Cell* **12,** 1367–1380 (2001).
12. Pelham, R. J. & Chang, F. Actin dynamics in the contractile ring during cytokinesis in fission yeast. *Nature* **419,** 82–86 (2002).
13. Wu, J. Q., Kuhn, J. R., Kovar, D. R. & Pollard, T. D. Spatial and temporal pathway for assembly and constriction of the contractile ring in fission yeast cytokinesis. *Dev. Cell* **5,** 723–734 (2003).
14. Arai, R. & Mabuchi, I. F-actin ring formation and the role of F-actin cables in the fission yeast Schizosaccharomyces pombe. *J. Cell Sci.* **115,** 887–898 (2002).
15. Kamasaki, T., Osumi, M. & Mabuchi, I. Three-dimensional arrangement of F-actin in the contractile ring of fission yeast. *J. Cell Biol.* **178,** 765–771 (2007).
16. Mabuchi, I. & Okuno, M. The effect of myosin antibody on the division of starfish blastomeres. *J. Cell Biol.* **74,** 251–263 (1977).
17. Straight, A. F. *et al.* Dissecting temporal and spatial control of cytokinesis with a myosin II Inhibitor. *Science* **299,** 1743–1747 (2003).
18. Nakamura, M., Kakuda, T., Oba, Y., Ojika, M. & Nakamura, H. Synthesis of biotinylated xestoquinone that retains inhibitory activity against Ca^{2+} ATPase of skeletal muscle myosin. *Bioorg. Med. Chem.* **11,** 3077–3082 (2003).
19. Kitayama, C., Sugimoto, A. & Yamamoto, M. Type II myosin heavy chain encoded by the myo2 gene composes the contractile ring during cytokinesis in Schizosaccharomyces pombe. *J. Cell Biol.* **137,** 1309–1319 (1997).
20. Motegi, F., Nakano, K., Kitayama, C., Yamamoto, M. & Mabuchi, I. Identification of Myo3, a second type-II myosin heavy chain in the fission yeast Schizosaccharomyces pombe. *FEBS Lett.* **420,** 161–166 (1997).
21. Bezanilla, M., Forsburg, S. L. & Pollard, T. D. Identification of a second myosin-II in Schizosaccharomyces pombe: Myp2p is conditionally required for cytokinesis. *Mol. Biol. Cell* **8,** 2693–2705 (1997).
22. Balasubramanian, M. *et al.* Isolation and characterization of new fission yeast cytokinesis mutants. *Genetics* **149,** 1265–1275 (1998).
23. Lord, M. & Pollard, T. D. UCS protein Rng3p activates actin filament gliding by fission yeast myosin-II. *J. Cell Biol.* **167,** 315–325 (2004).
24. Wong, K. C., Naqvi, N. I., Iino, Y., Yamamoto, M. & Balasubramanian, M. K. Fission yeast Rng3p: An UCS-domain protein that mediates myosin II assembly during cytokinesis. *J. Cell Sci.* **113,** 2421–2432 (2000).
25. McCollum, D., Balasubramanian, M. K., Pelcher, L. E., Hemmingsen, S. M. & Gould, K. L. Schizosaccharomyces pombe $cdc4^{+}$ gene encodes a novel EF-hand protein essential for cytokinesis. *J. Cell Biol.* **130,** 651–660 (1995).
26. Mendes Pinto, I., Rubinstein, B., Kucharavy, A., Unruh, J. R. & Li, R. Actin depolymerization drives actomyosin ring contraction during budding yeast cytokinesis. *Dev. Cell* **22,** 1247–1260 (2012).
27. Nakano, K. & Mabuchi, I. Actin-depolymerizing protein Adf1 is required for formation and maintenance of the contractile ring during cytokinesis in fission yeast. *Mol. Biol. Cell* **17,** 1933–1945 (2006).
28. Kovar, D. R., Kuhn, J. R., Tichy, A. L. & Pollard, T. D. The fission yeast cytokinesis formin Cdc12p is a barbed end actin filament capping protein gated by profilin. *J. Cell Biol.* **161,** 875–887 (2003).
29. Chang, F., Drubin, D. & Nurse, P. cdc12p, a protein required for cytokinesis in fission yeast, is a component of the cell division ring and interacts with profilin. *J. Cell Biol.* **137,** 169–182 (1997).
30. Roberts-Galbraith, R. H. *et al.* Dephosphorylation of F-BAR protein Cdc15 modulates its conformation and stimulates its scaffolding activity at the cell division site. *Mol. Cell* **39,** 86–99 (2010).
31. Balasubramanian, M. K., Helfman, D. M. & Hemmingsen, S. M. A new tropomyosin essential for cytokinesis in the fission yeast S. pombe. *Nature* **360,** 84–87 (1992).
32. Stark, B. C., Sladewski, T. E., Pollard, L. W. & Lord, M. Tropomyosin and myosin-II cellular levels promote actomyosin ring assembly in fission yeast. *Mol. Biol. Cell* **21,** 989–1000 (2010).
33. Eng, K., Naqvi, N. I., Wong, K. C. & Balasubramanian, M. K. Rng2p, a protein required for cytokinesis in fission yeast, is a component of the actomyosin ring and the spindle pole body. *Curr. Biol.* **8,** 611–621 (1998).
34. Nakano, K., Satoh, K., Morimatsu, A., Ohnuma, M. & Mabuchi, I. Interactions among a fimbrin, a capping protein, and an actin-depolymerizing factor in organization of the fission yeast actin cytoskeleton. *Mol. Biol. Cell* **12,** 3515–3526 (2001).
35. Takaine, M., Numata, O. & Nakano, K. Fission yeast IQGAP arranges actin filaments into the cytokinetic contractile ring. *EMBO J.* **28,** 3117–3131 (2009).

© 2013 Macmillan Publishers Limited. All rights reserved.

DOI: 10.1038/ncb2781

METHODS

Strains, genetic techniques, chemicals and spheroplasting. *S. pombe* strains used in this study are listed in Supplementary Table S5. Standard procedures for *S. pombe* genetics were used[36]. Blebbistatin and Jasp were purchased from Calbiochem and CytA, MBC and TBZ were purchased from Sigma. Strains expressing epitope-tagged proteins were constructed using a PCR-based approach[37]. Spheroplasts were obtained as described previously[9,38]. The use of a synchronous cell culture of *cdc25*-22 cells carrying Rlc1–3xGFP enhanced the proportion of spheroplasts and cell ghosts with a contractile ring. Cells were first grown at the permissive temperature of 25 °C to early log phase in minimal medium containing 0.5% glucose. These cells were then shifted to the restrictive temperature of 36 °C for 4 h before spheroplasting. The time for cell wall digestion was different among various strains and varied from 20 min to a 1 h. Typically more than 90% of the cells were spheroplasted in all experiments. These spheroplasts were then grown in minimal medium with 0.8% sorbitol at 25 °C with slow shaking (80 r.p.m.). Contractile ring formation was monitored by fluorescence microscopy. For a typical experiment, at the point of spheroplasting Rlc1–3xGFP signal was detected in a single bright dot-like structure in 100% of the spheroplasts and actomyosin arcs or contractile rings were not seen. After 5 h of incubation at 24 °C, actomyosin arcs could be detected (in 3–7% of cells) and 25–35% of the spheroplasts had a fully formed contractile ring. At this point spheroplasts were collected for permeabilization and the analysis of the contraction competence of arcs and rings is described in the manuscript. For preparation of cell ghosts from various cytokinesis mutants, mutant cells expressing Rlc1–3GFP or Rlc1–GFP were grown at the permissive temperature of 25 °C overnight in minimal medium containing 0.5% glucose and spheroplasted at 25 °C. To determine the time taken for inactivation of various ts mutant proteins, intact mutant cells were shifted to the restrictive temperature of 36 °C and their inability to compact the contractile ring was monitored.

Permeabilization of spheroplasts and preparation of cell ghosts. Spheroplasts were washed twice with wash buffer (0.8 M sorbitol, 2 mM EGTA, 5 mM $MgCl_2$ and 20 mM PIPES–NaOH, at pH 7.0) and incubated for 5 min in isolation buffer (0.16 M sucrose, 50 mM EGTA, 5 mM $MgCl_2$, 50 mM potassium acetate, 50 mM PIPES–NaOH, at pH 7.0, 0.5% NP-40, 10 μg ml^{-1} leupeptin, 10 μg ml^{-1} aprotinin, 10 μg ml^{-1} pepstatin, 0.5 mM phenylmethylsulphonyl fluoride and 1 mM dithiothreitol) on ice. Spheroplasts were homogenized with a Teflon/glass homogenizer. Cell ghosts were washed twice with reactivation buffer (0.16 M sucrose, 5 mM $MgCl_2$, 50 mM potassium acetate, 20 mM MOPS–NaOH, at pH 7.0, 10 μg ml^{-1} leupeptin, 10 μg ml^{-1} aprotinin, 10 μg ml^{-1} pepstatin, 0.5 mM phenylmethylsulphonyl fluoride and 1 mM dithiothreitol). About 30% of the resultant cell ghosts retained intact contractile rings and another 5–10% had actomyosin arcs or discontinuous or fragmented contractile rings. Most intact fully formed contractile rings were competent for *in vitro* contraction on ATP addition.

Protein localization in cell ghosts and immunofluorescence microscopy. Cell ghosts were prepared from strains carrying the protein of interest fused to fluorescent proteins as described above. Indirect immunofluorescence was used to label Cdc4p and Adf1p. F-actin was stained with BODIPY-FL–phallacidin, Alexa 568–phalloidin (Molecular Probes-Invitrogen) or synthesized tetramethylrhodamine-labelled Lifeact peptide (Operon Biotechnologies). For immunofluorescence microscopy, cell ghosts were fixed with 3.8% paraformaldehyde in PEM buffer (1 mM EGTA, 1 mM $MgCl_2$ and 0.1 M PIPES–NaOH, at pH 6.9) for 30 min. After washing with PEM buffer, cell ghosts were blocked in PEM buffer containing 1% BSA, 0.1% NaN_3 and 10 mM L-lysine-HCl for 1 h at room temperature. Rabbit anti-Cdc4 polyclonal antibody[25] (1:100) and rabbit anti-Adf1 (ref. 27) polyclonal antibody (1:500) were used as a primary antibody for Cdc4p and Adf1p detection, respectively. Tetramethylrhodamine-conjugated anti-rabbit IgG was used as a secondary antibody at 1:1,000.

Electron microscopy. Cell ghosts for electron microscopy were prepared as described previously[39]. Actin filaments were decorated with skeletal heavy meromyosin for easy visualization. Sections were examined with a JEM1400 electron microscope (JEOL) at 80–100 kV.

Reactivation of contractile ring and microscopy. The reactivation of the contractile ring in the cell ghost was assessed with a hand-made perfusion chamber. The base of the chamber was constructed with a large coverslip (Matsunami Glass, 24 × 36 mm, No.1) coated with 0.01% poly-L-Lysine (Sigma, P1524) and double-sided tape (Nichiban; NW-5S, 60 μm wall thickness). Cell ghosts in suspension were adhered to the base of the chamber and then covered with a small coverslip (Matsunami, 18 × 18 mm, No. 1). The volume in the chamber was around 10 μl. Cell ghosts were washed with reactivation buffer by perfusion. Reactivation was performed by perfusion with reactivation buffer containing an appropriate concentration of ATP. Most intact contractile rings in wild-type cell ghosts underwent ATP-mediated contraction.

Conventional fluorescence microscopy, three-dimensional reconstruction and time-lapse observations were made using a DeltaVision system (Applied Precision) attached to an Olympus IX-70 wide-field inverted fluorescence microscope equipped with an Olympus UplanSApo ×100 oil-immersion objective lens (NA 1.4, Olympus), and a Photometrics CoolSNAP HQ camera (Roper Scientific). Temperature was controlled by both the thermo-plate and a lens heater (MATS-55RAF20, MATS-LH; TOKAI HIT). More than 14 optical sections (0.5 μm spaces) were acquired every 10 s. Images were captured and processed by iterative constrained deconvolution using SoftWoRx (Applied Precision), and analysed by SoftWoRx and ImageJ (W. S. Rasband, National Institutes of Health, Bethesda, MD) incorporated with the McMaster Biophotonics Facility ImageJ for Microscopy collection of plugins (T. Collins, McMaster Biophotonics Facility, Hamilton, Ontario, Canada). For measurement of the contraction rate, stacks of optical sections were reconstructed in a horizontal direction using the three-dimensional rotation tool of SoftWoRx and the perimeter of each ring was measured. Each contraction rate was determined by using values of the most linear phase of contraction. For measurement of fluorescence intensity in Fig. 4b, sum projections of six deconvolved sections were used. Integrated intensity was calculated from mean value and area, after subtracting the background mean value of the same area. Graphical images were established using Prism-5 (Graphpad Software).

Actin disassembly assay and western blotting. Cell ghosts suspended in reactivation buffer were split into three. A half-volume of reactivation buffer containing 15% dimethylsulphoxide or 0.3 mM Jasp was added and gently mixed. After three minutes, a one-quarter volume of reactivation buffer containing 5% dimethylsulphoxide, 5% dimethylsulphoxide and 2 mM ATP, or 0.1 mM Jasp and 2 mM ATP was added and gently mixed to induce ring contraction. After five minutes incubation at 25 °C, suspensions were centrifuged at 16,000*g* for 5 min at 4 °C. The pellet was frozen at −80 °C. Supernatant with 0.02% deoxycholate added was left for 30 min on ice followed by 10% trichloroacetic acid addition and overnight incubation on ice. Precipitates were washed with cold acetone and dried. The pellet and supernatant were analysed by SDS–PAGE and western blotting. The volume of pellet loaded was one-third that of the supernatant. For the sedimentation assay, half of the supernatant was centrifuged at 200,000*g* for 15 min at 4 °C. As primary antibody, mouse anti-actin monoclonal antibody MAB1501 (1:1,000, Millipore), rabbit anti-GFP polyclonal antibody 598 (1:2,000, MBL), rabbit anti-Cdc8 polyclonal antibody (1:250; ref. 40) or mouse anti-α-tubulin monoclonal antibody TAT-1 (1:1,000, gift from K. Gull) was used. Appropriate HRP-conjugated secondary antibody was used at 1:5,000. Western blots were developed using SuperSignal West Pico Chemiluminescent Substrate (Thermo Fisher Scientific, Waltham) and luminoimage analyser LAS3000 (Fujifilm). Each integrated intensity was calculated from the mean value and the area measured using ImageJ.

Measurement of ATPase activity. Motor proteins used were a mixture of rabbit skeletal muscle myosin chymotryptic S1 (0.18 mg ml^{-1}) and rabbit skeletal muscle F-actin (0.89 mg ml^{-1}), sea urchin sperm axonemal dynein (Tris–EDTA extract, 0.21 mg ml^{-1}), and recombinant rat brain kinesin-1 motor domain (relative molecular mass 430,000, 0.17 mg ml^{-1}, gift from Y. Toyoshima). These were incubated in 0.1 M KCl, 2.8 mM $MgCl_2$, 10 mM TES (pH 7.0) and 2.6 mM ATP at 25 °C. EDTA (0.55 mM) was also included for dynein and kinesin. Inorganic phosphates released were measured by the method of ref. 41 after removing proteins as trichloroacetic-acid-induced precipitates.

Statistical analysis. Statistical comparisons of mean values were made using the unpaired two-tailed *t*-test for two data sets and one-way analysis of variance for multiple data sets. The actual *P* values for each test are represented in each figure.

36. Moreno, S., Klar, A. & Nurse, P. Molecular genetic analysis of fission yeast Schizosaccharomyces pombe. *Methods Enzymol.* **194,** 795–823 (1991).
37. Bähler, J. *et al.* Heterologous modules for efficient and versatile PCR-based gene targeting in Schizosaccharomyces pombe. *Yeast* **14,** 943–951 (1998).
38. Kobori, H., Yamada, N., Taki, A. & Osumi, M. Actin is associated with the formation of the cell wall in reverting protoplasts of the fission yeast Schizosaccharomyces pombe. *J. Cell Sci.* **94,** 635–646 (1989).
39. Kamasaki, T., Arai, R., Osumi, M. & Mabuchi, I. Directionality of F-actin cables changes during the fission yeast cell cycle. *Nat. Cell Biol.* **7,** 916–917 (2005).
40. Arai, R., Nakano, K. & Mabuchi, I. Subcellular localization and possible function of actin, tropomyosin and actin-related protein 3 (Arp3) in the fission yeast Schizosaccharomyces pombe. *Eur. J. Cell Biol.* **76,** 288–295 (1998).
41. Fiske, C. H. & Subbarow, Y. The Colorimetric determination of phosphorus. *J. Biol. Chem.* **66,** 375–400 (1925).

© 2013 Macmillan Publishers Limited. All rights reserved.

DOI: 10.1038/ncb2781

nature cell biology

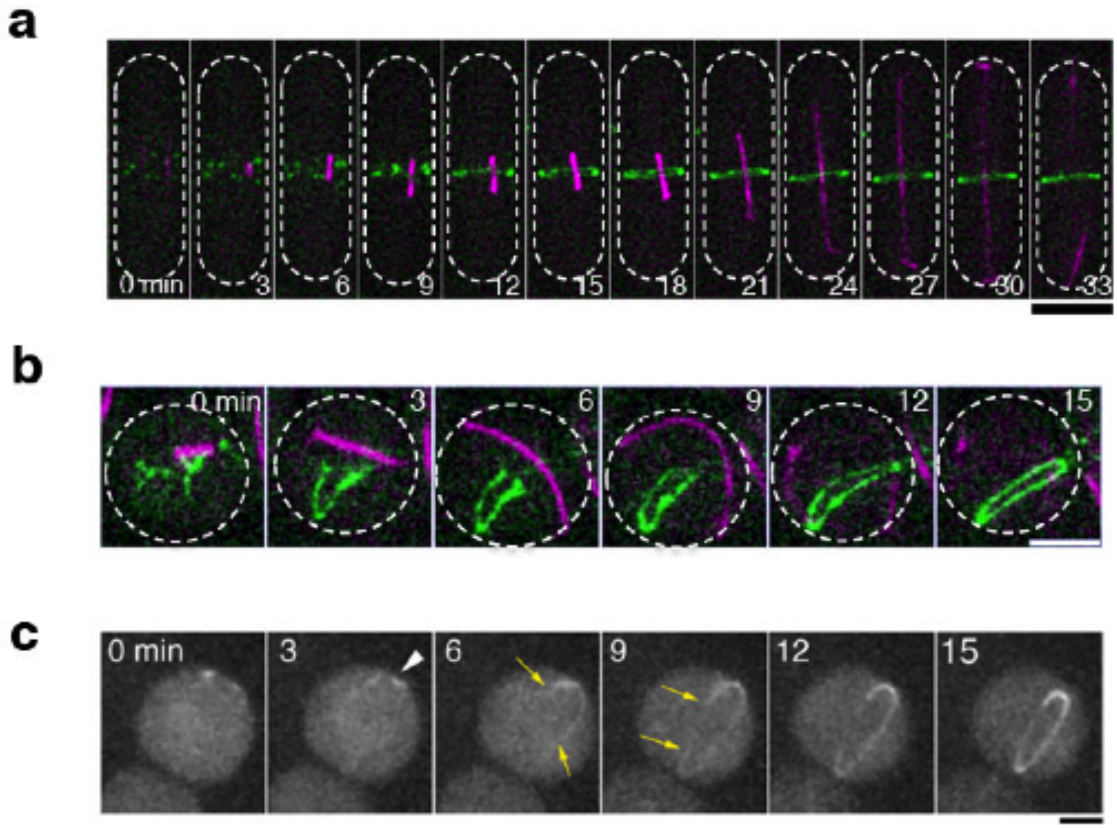

Figure S1 Examples of contractile ring formation in intact wild type cell, spheroplast and spherical mutant. (**a**) Maximum projections of deconvolved sections of Rlc1-3xGFP and mCherry-Atb2 images in an intact fission yeast cell. White doted lines indicate the cell outline. (**b**) Maximum projections of deconvolved sections of Rlc1-3xGFP and mCherry-Atb2 images in an intact spheroplast. White dotted line represents the outline of the spheroplast. (**c**) Maximum projections of contractile ring formation in *orb3/nak1* null cell (*orb3*Δ) expressing Rlc1-3xGFP at 25˚C. Contractile ring initiates from one predominant location on the surface of the spheroplast (shown by arrowhead at time 0 min) and grows in a bidirectional manner (shown by yellow arrows) to form a mature ring. Scale bars, 5 μm.

© 2013 Macmillan Publishers Limited. All rights reserved.

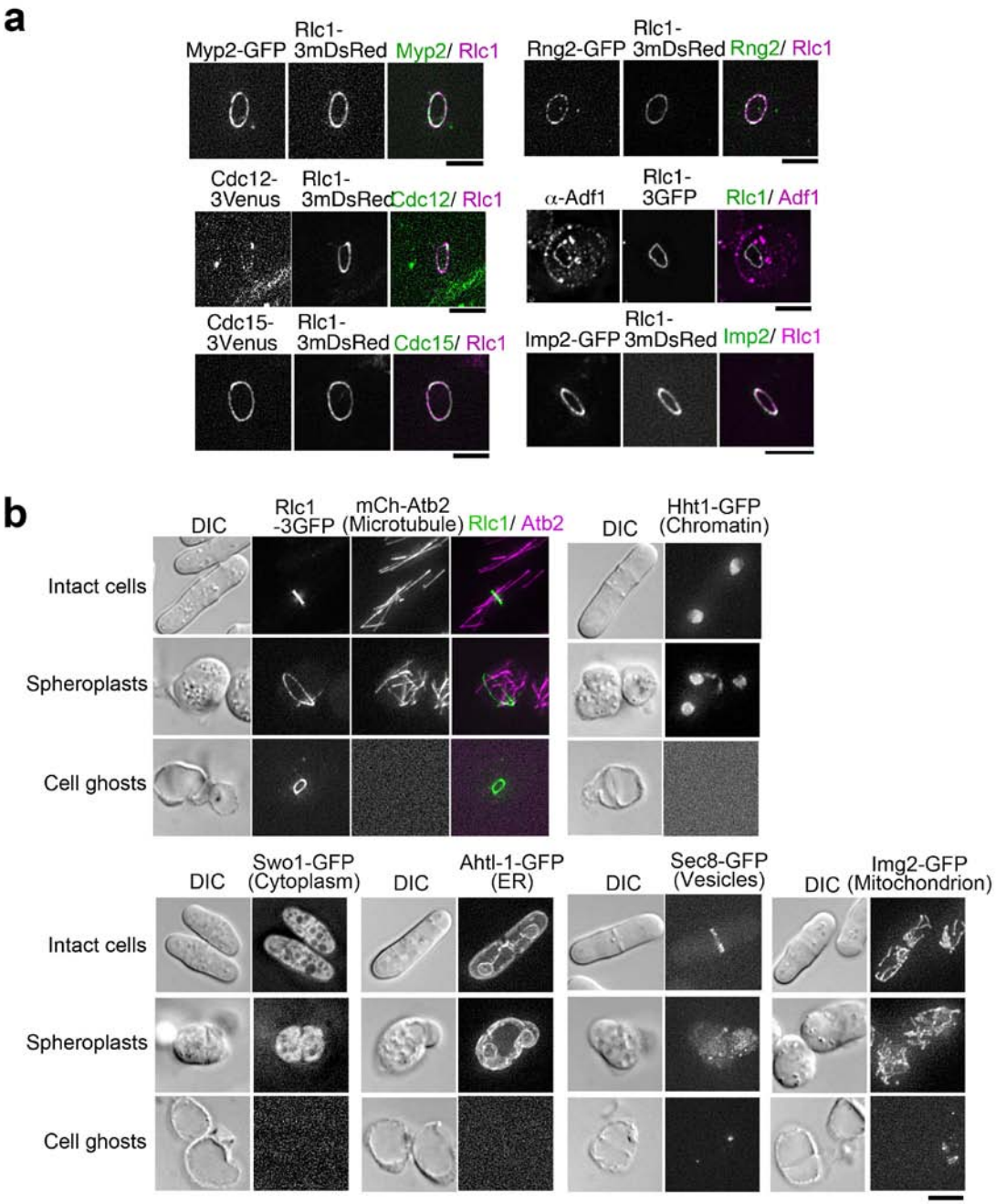

Figure S2 Cell-ghosts contain essential contractile ring proteins but lack other cytoplasmic components. (**a**) Essential components of the contractile ring are retained in cell-ghosts. Images are shown as maximum projections of Z-stacks. Spheroplasts expressing fluorescent-tagged proteins as indicated on each image were permeabilised before imaging. Adf1 was stained with anti-Adf1 antibody and anti-rabbit IgG labeled with tetramethylrhodamine after permeabilisation of spheroplasts expressing Rlc1-3xGFP. (**b**) Most cytoplasmic components are not retained in cell-ghosts. Fluorescence images are shown as maximum projections of deconvolved sections. Spheroplasts expressing fluorescent-tagged proteins as indicated were imaged before and after permeabilisation. Scale bars, 5 μm.

© 2013 Macmillan Publishers Limited. All rights reserved.

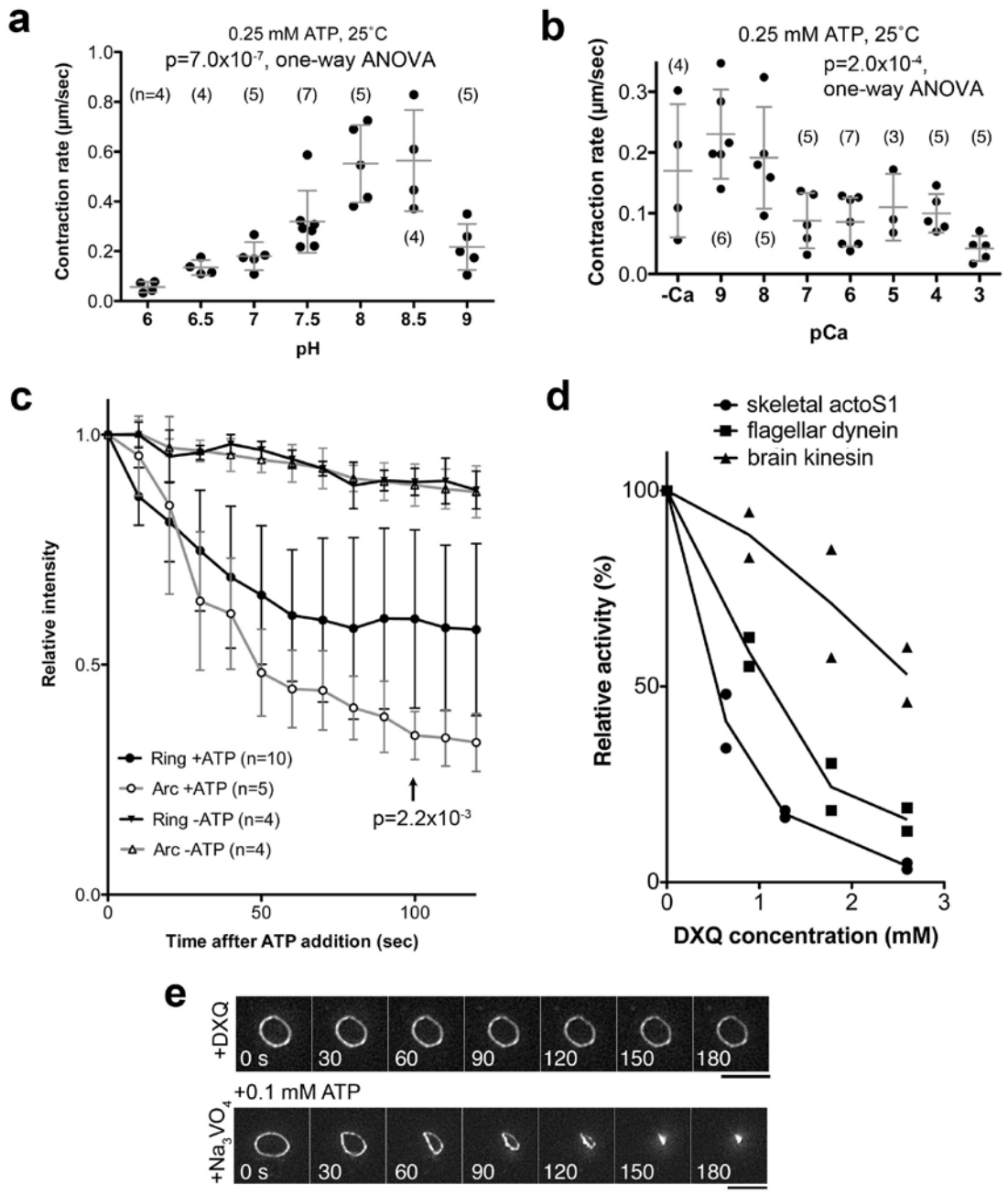

Figure S3 General features and myosin ATPase dependency of ring contraction *in vitro.* Experiments were done at 25˚C. (**a**) pH sensitivity of ring contraction *in vitro.* ATP concentration was 0.25 mM. Each spot represents the rate of contraction of an individual ring. Medial horizontal lines and error bars represent mean values and standard deviations, respectively. One-way analysis of variance (ANOVA) was used for statistical analysis. See Table S6 for statistics source data. (**b**) Ca^{++} sensitivity of ring contraction *in vitro.* ATP concentration was 0.25 mM. Statistical analysis in panel b was done as in panel a. See Table S6 for statistics source data. (**c**) Reduction of relative fluorescence intensity after 0.5 mM ATP addition. Integrated fluorescence was calculated from mean values of area of region of interest and were normalised to the value at time 0. It is apparent that the photobleaching and/or spontaneous loss of Rlc1-3GFP from contractile ring or from the arc in the absence of ATP are relatively minor. (**d**) Effect of dehydroxestoquinone (DXQ) on ATPase activity of motor proteins. DXQ has been reported to be an ATPase inhibitor that inhibits ATPase activity of muscle myosin II. Since DXQ had not been tested on other ATPase-motors, we tested its effects on kinesin (from brain), dynein (flagella), and myosin II S1 fragment (skeletal muscle) as a control. DXQ showed strong inhibition of ATPase activity of myosin II and dynein and a weaker inhibition of kinesin. Mean values of two measurements are plotted. See Table S6 for statistics source data. (**e**) Ring contraction was inhibited by the addition of 2.5 mM DXQ. Vanadate, which at 100 μM inhibits kinesin and dynein ATPases, did not affect ring contraction. Fluorescent images of Rlc1-3xGFP are shown as maximum projections of Z-stacks (0.5 μm spaces). ATP concentration was 0.5 mM for DXQ or 0.1 mM for vanadate. Scale bar, 5 μm.

© 2013 Macmillan Publishers Limited. All rights reserved.

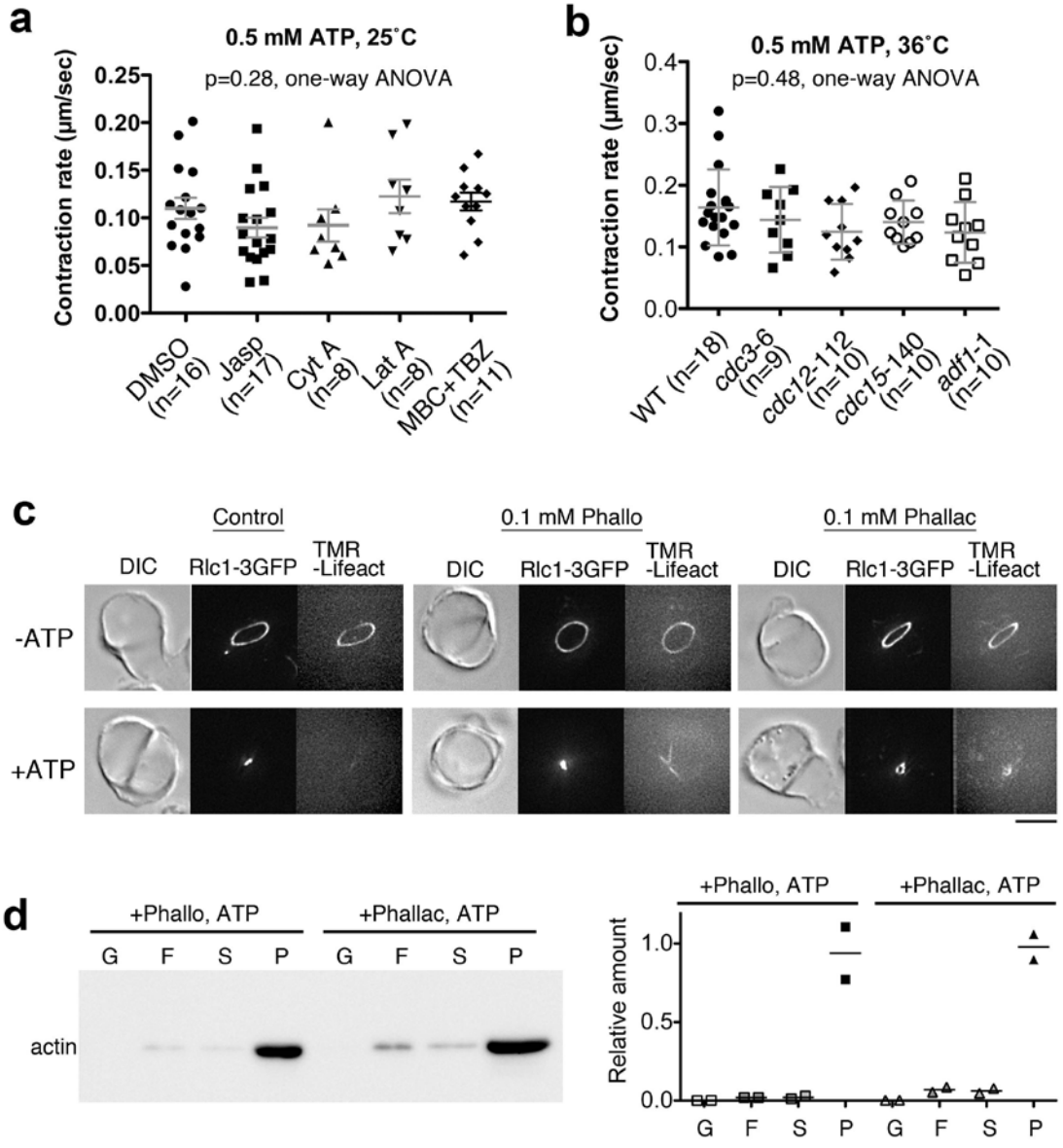

Figure S4 Neither actin polymerization nor depolymerization are required for ring contraction *in vitro*. (**a**) The effects of drugs (Jasp, 0.1 mM jasplakinolide; Cyt A, 0.1 mM cytochalasin A; Lat A, 10 μM latrunculin A; MBC+TBZ, 50 μg/ml MBC and 50 μg/ml TBZ) on ring contraction *in vitro*. 5% dimethyl sulfoxide (DMSO) was used for control experiment. Each spot represents the rate of contraction of an individual ring. Medial horizontal lines and error bars represent mean values and standard deviations, respectively. (**b**) 0.5 mM ATP was added after appropriate incubation at 36˚C (*cdc3*-6^{ts}, 20 min.; *cdc12*-112^{ts} *cdc15*-140^{ts} and *adf1*-1^{ts}, 15 min). Wild-type cell-ghosts were incubated at 36˚C for 30-40 minutes before ATP addition. A graphical representation of the data is shown. (**c**) Phalloidin and phallacidin prevent release of actin from contractile ring after ATP addition. Actin was stained with 10 μg/ml TMR-Lifeact before or after contraction. Fluorescent images of Rlc1-3xGFP and TMR-Lifeact are shown as maximum projections of Z-stacks (0.5 μm steps). Scale bar, 5 μm. (**d**) Western blot analysis of actin disassembly upon ATP addition in the presence of phalloidin or phallacidin. S, supernatant; P, pellet; G, G-actin and short F-actin; F, F-actin. Each relative amount was calculated from the amount of actin in the pellet without ATP. Each spot represents relative amount in individual experiment. See Table S6 for statistics source data. See also Fig. 4c, f.

© 2013 Macmillan Publishers Limited. All rights reserved.

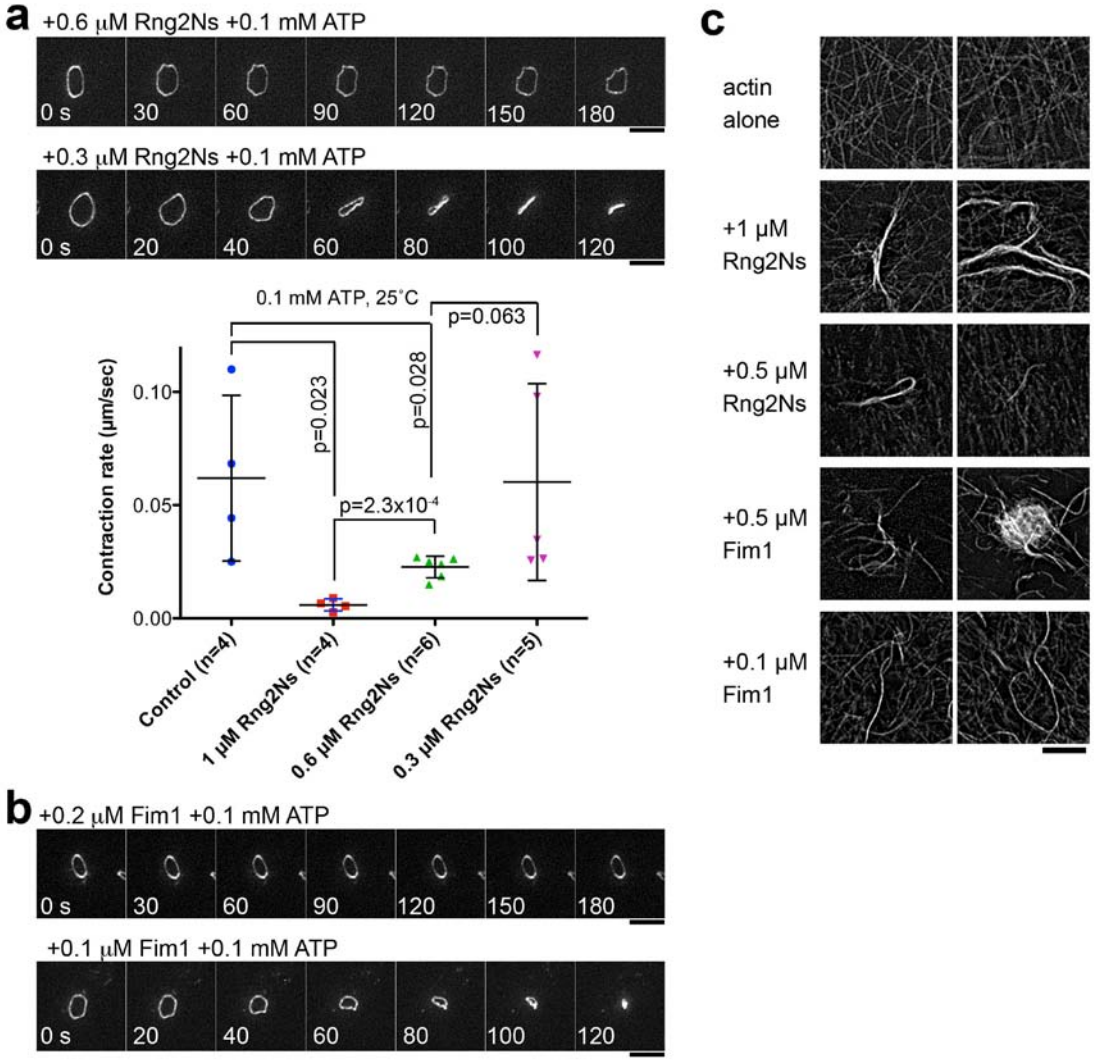

Figure S5 Dose dependent inhibition of ring contraction by purified actin-bundling proteins *in vitro*. (**a**-**b**) Cell-ghosts were incubated in the presence of purified proteins at the indicated concentrations for 3 minutes before addition of 0.1 mM ATP. Experiments were done at 25˚C. Fluorescent images of Rlc1-3xGFP are shown as maximum projections of Z-stacks (0.5 μm steps). Each spot represents the rate of contraction of an individual ring. Medial horizontal lines and error bars represent mean values and standard deviations, respectively. See Table S6 for statistics source data. (**c**) Actin-cross-linking activities of purified actin- bundling proteins. Skeletal actin (3 μM) was polymerised in the reactivation buffer including purified proteins for 30 minutes at room temperature. F-actin was stained with BODIPY-FL-phallacidin. Both, 1 μM Rng2Ns and 0.5 μM Fim1 show robust actin-bundling activity. Images are deconvolved from single focal planes. Scale bars, 5 μm.

© 2013 Macmillan Publishers Limited. All rights reserved.

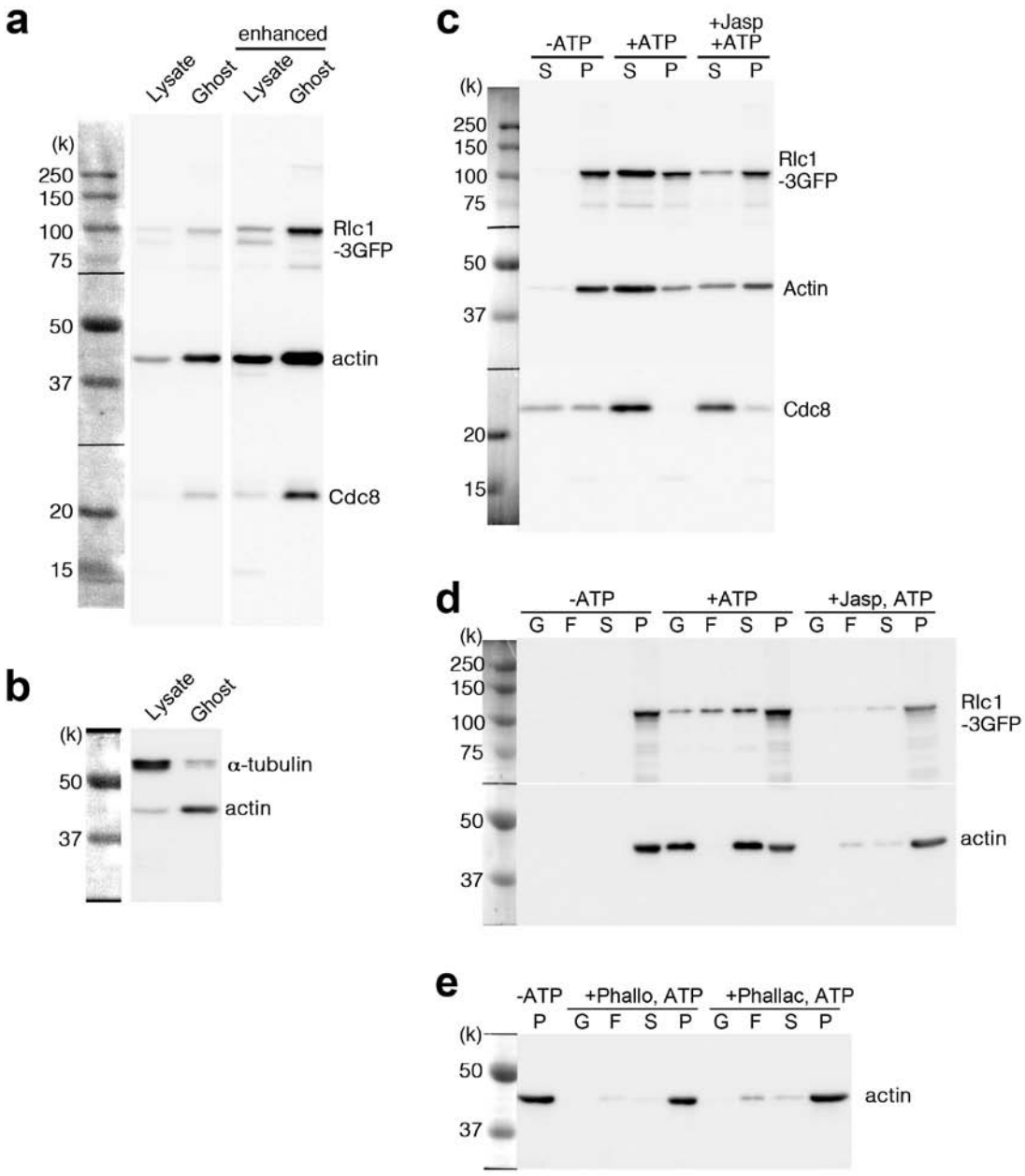

Figure S6 Full scans of original blots. (**a-b**) Full scan of blot shown in Fig. 1 h. (**c**) Full scan of blot shown in Fig. 4 d-e. (**d**) Full scan of blot shown in Fig. 4 f. (**e**) Full scan of blot shown in Fig. S4d.

© 2013 Macmillan Publishers Limited. All rights reserved.

Supplementary Table Legends:

Table S1. Proteins in the contractile rings. Intact cells and cell-ghosts expressing fluorescent-tagged proteins as indicated were imaged. Indirect immunoflurosence was used to label Cdc4p and Adf1p. Actin was detected by Alexa 568- phalloidin.

Table S2. *P* values for comparison of relative intensities of contractile ring components in Fig. 2f. Values at 100 seconds were compared. Unpaired two-tailed t-test was used for this analysis. *P* values less than 0.05, are represented in bold.

Table S3. Contraction rates in various nucleotide concentrations. Mean±SD was indicated. These datasets were used for the graph shown in Fig. 2h and calculation of K_m and V_m in Fig. 2i.

Table S4. Contractile ring components in the mutant rings. Cell-ghosts were prepared from the mutant cells expressing the indicated fluorescent-tagged proteins. Cell-ghosts were incubated at restrictive temperature to inactivate the mutant protein before imaging. Indirect immunofluorescence was used to label Cdc4p

Table S5. List of strains used in this study. *YGRC, Yeast Genetic Resource Center Japan. (http://yeast.lab.nig.ac.jp/nig/index_en.html).

Supplementary Video Legends:

Video S1. ATP drives ring contraction *in vitro*. The video of a contracting ring in the presence of 0.5 mM ATP at 25˚C corresponds to the frames shown in Fig. 2**a**. X-Y and Y-Z images were shown as non-tilted and 90˚-tilted maximum projections of Z-stacks, respectively.

Video S2. ATP drives ring contraction. The video of a contracting ring in the presence of 0.01 mM ATP at 25˚C corresponds to the frames shown in Fig. 2**c**. X-Y and Y-Z images were shown as non-tilted and 90˚-tilted maximum projections of Z-stacks, respectively.

Video S3. AMP-PNP does not induce ring contraction *in vitro*. Experiment was done at 25˚C. The video corresponds to the frames shown in Fig. 2**d**. X-Y and Y-Z images were shown as non-tilted and 90˚-tilted maximum projections of Z-stacks, respectively.

Video S4. The plasma membrane of Rlc1-3xGFP expressing cell-ghosts stained with FM4-64 during contraction *in vitro*. Experiment was done at 25˚C. The membrane did not ingress as the ring contracts. The video corresponds to the frames shown in Fig. 2**g**.

Video S5. Incomplete actomyosin arcs do not show ATP-dependent contraction *in vitro*. The GFP fluorescence decays the presence of 0.5 mM ATP but the actomyosin arc do not show any contraction at 25˚C. The video corresponds to the frames shown in Fig. 2**j**. X-Y and Y-Z images were shown as non-tilted and 90˚-tilted maximum projections of Z-stacks, respectively

Video S6. Contractile ring of *myo2*-E1^{ts} undergoes slow *in vitro* contraction even at the permissive temperature of 25˚C. The video corresponds to the frames shown in Fig. 3**b**.

Video S7. Contractile ring of *myp2* null mutant (*myp2*Δ) *in vitro*. Experiment was done at 25˚C. The video corresponds to the frames shown in Fig. 3**b**.

Video S8. Contractile ring contraction of the double mutant of *myo2* and *myp2* (*myo2*-E1^{ts} *myp2*Δ) *in vitro*. These rings did not show any contraction and instead fragmented and disassembled in presence of ATP at 25˚C. The video corresponds to the frames shown in Fig. 3**b**.

Video S9. Addition of Jasplakinolide does not affect ring contraction *in vitro*. Experiment was done at 25˚C.

Video S10. ADF/cofilin (Adf1p) is not required for ring contraction *in vitro*. Cell-ghosts from *adf1*-1^{ts} were held at 36˚C for 15 minutes before ATP addition.

Video S11. LatA has minimal effect on ring contraction *in vitro*. Experiment was done at 25˚C.

Video S12. Formin (Cdc12p) is not required for ring contraction *in vitro*. Experiment was done at 36˚C. Cell-ghosts from *cdc12*-112^{ts} were held at 36˚C for 15 minutes before ATP addition.

Video S13. F-BAR protein (Cdc15p) is not required for ring contraction *in vitro*. Experiment was done at 36˚C. Cell-ghosts from *cdc15*-140^{ts} were held at 36˚C for 15 minutes before ATP addition.

Video S14. Tropomyosin (Cdc8p) is required for integrity and contraction of ring *in vitro*. Cell-ghosts from *cdc8*-110^{ts} were held at 36˚C for 15 minutes before ATP addition. The video corresponds to the frames shown in Fig. 5**a**.

Video S15. Addition of 1 μM purified N-terminal region of IQGAP (Rng2Ns) completely blocks ring contraction *in vitro*. Experiment was done at 25˚C. The video corresponds to the frames shown in Fig. 5**b**.

Video S16. Addition of 0.9 μM purified fimbrin (Fim1p) completely blocks ring contraction *in vitro*. Experiment was done at 25˚C. The video corresponds to the frames shown in Fig. 5**c**.

© 2013 Macmillan Publishers Limited. All rights reserved.